Nanocoating on cotton fabric with nitrogen-doped graphene quantum dots/titanium dioxide/PVA: An erythemal UV protection and photoluminescent finishing

B. H. S. Felipe[1*], R. L. B. Cabral[2,3*], R. Ladchumananandasivam[1], A. Zille[5], S. Kim[6], P. B. A. Fechine[7], J. H. O. Nascimento[1,2,3,4*]

[1]Graduate Program in Mechanical Engineering, Center of Technology, Natal –RN, Brazil. Federal University of Rio Grande do Norte, Av. Sen. Salgado Filho, 3000, CEP 59072-970 Natal, RN, Brazil.
[2]Graduate Program in Textile Engineering, Center of Technology, Natal –RN, Brazil. Federal University of Rio Grande do Norte, Av. Sen. Salgado Filho, 3000, CEP 59072-970 Natal, RN, Brazil.
[3]Research Group on Innovation in Micro and Nanotechnology - Department of Textile Engineering, Federal University of Rio Grande do Norte, Av. Sen. Salgado Filho, 3000, CEP 59072-970 Natal, RN, Brazil.
[4]Department of Textile Engineering, Center of Technology, Natal –RN, Brazil. Federal University of Rio Grande do Norte, Av. Sen. Salgado Filho, 3000, CEP 59072-970 Natal, RN, Brazil.
[5]Centre for Textile Science and Technology, Department of Textile Engineering, University of Minho, 4800-058, Guimarães, Portugal
[6]Department of Engineering, Pontificia Universidad Católica del Perú PUCP, Av. Universitaria 1801, Lima 32, Peru
[7]Group of Chemistry of Advanced Materials (GQMat) - Department of Analytical Chemistry and Physical Chemistry, Science Center, Federal University of Ceará (UFC), Fortaleza - CE, Zip Code 60455-760, Brazil

E-mail: brennohenrique@yahoo.com.br, systemriva38@gmail.com, joseheriberto@ct.ufrn.br

Abstract

Prolonged exposure to ultraviolet (UV) radiation from the sun can result in several skin problems, such as accelerating aging, burns, blemishes, or even cancer. Even when wearing clothes, there is still a risk that the user will be exposed to UV radiation and suffer skin damage. Therefore, it is necessary to apply anti-UV treatments to the clothes and fabrics used, so that users become safe. Nitrogen doped graphene quantum dots (N-GQD) and titanium dioxide (TiO_2) NPs are materials that have a broad spectrum of UV absorption and are promising candidates to be applied in functional finishing in use on textile materials, giving textiles property anti-UV. The aim of this research is to evaluate the synergy effect between N-GQD and TiO_2 NPs in getting a nanocoating that can be applied on a cotton fabric, add photoluminescent and anti-UV properties. The nanocoatings obtained were applied via industrial discontinuous method, the high-pressure and high-temperature exhaustion process to the cotton fabric using polyvinyl alcohol as a binding agent. According to the UV protection assessment, it was observed that both materials are excellent UV absorbers and their ultraviolet protection factor (UPF) are highly dependent on the concentrations used in the nanocoated cotton fabrics. Thus, nanocoated cotton with TiO_2, N-GQD and TiO_2/N-GQD revealed an UPF of +50, which established their effectiveness in protecting against UV radiation. They also withstand up to 20 wash cycles with no change in UPF.

Keywords: Nitrogen doped; graphen quantum dots; titanium dioxide; UV protection; photoluminescence; PVA

1. Introduction

The solar radiation that passes through the earth's atmosphere has an electromagnetic spectrum with a wavelength of 290 to 3000 nm. The region corresponding to the wavelengths between 290-400 nm refers to the range of ultraviolet (UV) radiation, which, from the point of view of biologists, is divided into: UVA (400-320 nm), UVB (320-290 nm) and UVC (290-190 nm). Long-term exposure can result in a number of skin problems, such as accelerated aging, burns, blemishes, and specific illnesses that require you to stay out of sunlight, such as lupus erythematosus or even cancer. Thus, the protection of the body is essential in order to reduce these damages to health [1–4].

Specific sunscreens and clothing with a protection factor against UVA/UVB radiation have been researched and developed as they are essential to prevent extracellular, collagen degradation in the human body, DNA damage, chemical and histological changes in the epidermis and pathway activation of intracellular signaling involved in photoaging and photocarcinogenesis [5,6]. The degradation of the extracellular matrix results from the UVA radiation-induced production of matrix metalloproteinases (MMP) and activation of intracellular pathways in fibroblasts and keratinocytes. Particularly in keratinocytes, UVA radiation induces β-catenin nuclear translocation and stimulates MMP gene transcription [7,8]. And UVB-type radiation is primarily responsible for the development of skin cancer. UVC, although causing serious harm to human health, is completely absorbed by the earth's atmosphere [1,2]. Thus, prolonged exposure to the sun is one of the main factors for the risk of non-melanoma skin cancer (squamous cell carcinoma; basal cell carcinoma) and melanoma skin cancer (which forms in melanocytes), especially in childhood and adolescence, exposure to beds of tanning and family history of skin cancer [9].

In 2020, in the world, it was estimated 1.19 million of new cases of non-melanoma skin and 324713 cases of melanoma skin. The highest incidence rates of cancer of non-melanoma skins are found in Australia/New Zealand, North America and Western European countries for both men and women. For melanoma skin cancer, the highest incidences are in Australia and New Zealand as well as in Northern, Central and Eastern European countries [10]. A large part of the cases of skin cancer occurs due to not using sunscreen, excessive exposure to sun and artificial tanning in tanning beds, as well as people who are exposed to UV radiation in work environments or in outdoor activities without adequate protective clothing. Thus, medical science suggests that the use of sunscreen on the skin and clothing that absorbs ultraviolet radiation can help prevent this type of cancer [11,12]. Ultraviolet protection factor (UPF) is the scientific term used to quantify the ability of a fabric to prevent UV radiation from penetrating human skin. This numerical factor in a textile fabric is associated with its ability to absorb, reflect and/or scatter UV radiation, preventing light from crossing the fibrous barrier of the material and reaching human skin. However, pure textile do not provide an effective blockade of skin problem-inducing UV radiation. The UPF of a textile material depends on the synergy of all parameters selected for its manufacture and the conditions of use, including fabric coverage factor, fabric structure, fiber type, dyes or chemical treatments [13–15].

Cellulosic fibers that are biodegradable and environmentally friendly do not have double bonds in their chemical structure and therefore have a low UPF [16]. Thus, one

of the ways to increase the UPF of these cellulosic fibers is through functionalization using different types of chemical UV protection agents. Many studies have evaluated the action of NPs (NPs) in improving the UV protection properties of fabrics such as SiO_2, TiO_2, ZnO, CuO and Ag, applied by different types of physical or chemical methods [17,18]. TiO_2 is widely used as UV protecting agent in textiles due to its high efficiency, chemical stability, light resistance. The anatase and rutile phases of TiO_2 due to their gap energy (3.21 eV), are the most efficient for application in protection against UVA/UVB radiation. On the other hand, these NPs have a lower scattering effect in the region of visible, with little filtering of this region [19–22]. Furthermore, the International Agency for Research on Cancer (IARC) has classified TiO_2 NPs as a group 2B carcinogen, which limits their application in textile materials for use as UV protective agents [23–25].

Thus, one of the strategies to overcome this problem is to modify the TiO_2 NPs with carbonaceous nanostructured materials such as graphenes, forming a heterojunction, which has generated great interest from researchers for applications in UV protective textiles [26], antimicrobials [27] and self cleaning and biocompatible textile [28]. Lately, graphene quantum dots (GQDs) have been widely studied due to their easy obtainability by green synthesis, low toxicity and wide antibacterial and biomedical applications [23,29–31]. Its application on plastic and textile materials has been studied due to its high absorption in the UVA/UVB spectrum regions [32,33] and also evaluated its efficiency, stability and biocompatibility when doped with a heteroatom such as boron or nitrogen. This doping of GQDs provides high quantum yield, excellent UV absorption capacity, charge separation properties and inherits unique properties of graphene and quantum dots. In addition, it causes a greater surface area to volume ratio with delocalized electrons that favors drug loading efficiency through its π – π stacking interactions [34] and therefore, it is proven to be a biocompatible material with low toxicity even when evaluated with TiO_2 [35]. Few studies have been reported to date on the application of GQDs doped with heteroatoms. Only the one by Zuo et al. [36] who nanocoated cotton with GQDs co-doped with boron and nitrogen obtaining a protection factor of +30 and resistant to 20 washes.

Polyvinyl alcohol (PVA) has been widely used in the textile area due to its excellent properties as a binding agent and non-toxicity. PVA has a polyhydroxyl structure that has a high chemical affinity with the free hydroxyls present in cotton. Thus, hydrogen bonds can form between cotton and PVA. In addition, hydrogen bonds can also form between PVA molecules, leading to the formation of a thin film of PVA on the surface of cotton fibers

Therefore, this study evaluates the efficiency of UVA/UVB protection and photoluminescence of cotton fabric nanocoated with TiO_2, N-GQD and N-GQD/TiO_2 NPs. It also used PVA as a binding agent by the discontinuous method high-pressure and high-temperature (HP/HT) hydrothermal method, widely applied in the textile industry as well as the durability of its ultraviolet protection factor when subjected to domestic washing.

2. Material and methods

2.1. Synthesis of N-GQD

This synthesis procedure was based on various studies about citric acid carbonization [37–40]. For the synthesis of N-GQD, 1 mol of citric acid (Synth, PA) and 9 mol of urea (Synth, PA) were diluted in 10 ml of distilled water, stirred for 15 min on a shaking table at 150 rpm, sonicated for 15 min and heated for 90 min at 180 °C on a

hot plate. Then, NaOH (10 g/L) was added to the mixture until the pH remained around 8. The solution was centrifuged at 13000 rpm for 10 min and the supernatant was separated. Part of the supernatant was lyophilized to perform some characterizations.

2.2. Synthesis of TiO_2 NPs (NPs)

This synthesis procedure was based on an optimization study carried out by Behnajady, et al. [41]. 1 mol of titanium (IV) isopropoxide (Sigma Aldrich, 97%) was slowly dissolved in 1 mol of methanol (Isofar, P.A) under magnetic stirring. The solution obtained was sonicated for 1 h, then added to a reflux system with dropwise addition of water (65 moles) and magnetic stirring for 3 h at 80 °C. The sol phase obtained was dried and then calcined in a muffle for 3 h at 450°C. The obtained TiO_2 NPs solutions were naturally cooled and subsequently macerated until obtaining the powder.

2.3. Nanocoating cotton fabric

A cotton fabric (CO) donated by the company Vicunha AS (Brazil) was previously bleached. The bleaching was carried out by an oxidative process that consists of a bath with hydrogen peroxide (H_2O_2) (Synth, 50% puro), peroxide stabilizer (Golden Technology), NaOH (Synth, PA) and non-ionic detergent (Golden Technology). For every 1 g of cotton fabric, a 100 ml solution with 0.15 g of NaOH was used and 0.1 g of non-ionic detergente. Subsequently, the cotton fabric with the bleaching bath was shaken for 60 min at 80 °C on the hot plate. The fabric was neutralized with 0.1% acetic acid solution, washed and dried at 80 °C for 20 min.

The cotton fabric nanocoating was prepared in glass beakers with NPs solutions according to the concentrations shown in Table 1. The mixture was added in a sonicator where it was carried out for 2 h in an ultrasonic bath (SACCH-LITD30) at a frequency of 50 KHz, followed by stirring on a shaking table at 150 rpm for 30 min. Subsequently, all solutions were transferred with 2g of cotton fabrics in a hydrothermal machine (ALT-I / Mathis) in a bath ratio of 1:75. The nanocoating process remained for 150 min at 135 ºC and then 10% polyvinyl alcohol (PVA) (Dynamic, 80% hydrolyzed) was added over the bath volume. So, the process continued at 135 °C for another 150 min. After the nanocoating procedure, the fabrics were dried at 100 ºC for 2 h in a hot air dryer (LTE-MATHIS).

Table 1 - Formulations used for textile fabric nanocoated

Cod.	Sample	N-GQD (g/L)	TiO_2 (g)	Water (mL)
PC	PVA/CO	0	0	150
PTC	PVA/TiO_2/CO	0	0.278	150
PnGC	PVA/N-GQD/CO	0.1	0	150
PnGC1	PVA/N-GQD/CO	1	0	150
PTnGC	PVA/N-GQD/TiO_2/CO	0.1	0.278	150

2.4. Characterizations

Fourier transform infrared (FTIR) spectra of the samples were recorded using a VERTEX 70v FT-IR spectrometer (BRUKER, Billerica, MA, USA) with a resolution of 4 cm^{-1} and a spectral range of 4000-400 cm^{-1}. The X-ray diffraction (XRD) patterns were obtained in a Bruker / D2 PHASER diffractometer, with CuKα radiation and λ = 1.5418 Å, varying 2θ from 3º to 70º, with an angular pitch of 0.02º. Microstructural analysis via high resolution transmission microscopy (HRTEM) and selected area electronic diffraction (SAED) were performed with the JEM-2100 JEOL microscope operating at 200 kV and with a resolution of 0.2 nm and, nanocoated cotton fabrics

were characterized by field emission scanning electron microscopy / X-ray energy dispersive spectroscopy (FE-SEM/EDS) by Supra 35-VP, Carl Zeiss where the surface of the samples was treated with gold deposited on vacuum for 3 min. The surface morphology of the coated fabric samples was observed using an atomic force microscope (AFM) (Nanoscope IIIa, Digital Instruments, Santa Barbara, CA, USA) operating in non-contact mode. The swept area was between 1 x 1 μm^2 and 2 x 2 μm^2 and the topography was characterized by the root mean square of the deviations of the topographic profile in relation to a mean plane (R_{rms}) according to:

$$\boldsymbol{R_{rms=}}\left(\frac{\mathbf{1}}{\boldsymbol{L_xL_y}}\int_{\mathbf{0}}^{\boldsymbol{L_X}}\int_{\mathbf{0}}^{\boldsymbol{L_Y}}\boldsymbol{z^2(x,y)dxdy}\right)^{\mathbf{1/2}} \quad (1)$$

where *Lx* and *Ly* are the length of the sides of the mean plane and *z* are the mean height of the sample.

Chemical analysis on the surface of N-GQD and TiO_2 nanocoated fabric was performed by X-ray photoelectron spectroscopy (XPS) (VG Scientific ESCALAB 200A, Waltham, MA, USA) using a 15 kV AlKα monochromatic X-ray (300W). All binding energy (BE) values reported in the present work are with reference to the C1s carbon nucleus level at 284.6 eV. The curve fitting of the high-resolution spectra was performed with combined Gaussian-Lorentzian functions.

The color coordinates of the CIE (International Commission on Illumination) and reflectance spectra of the samples were determined with a KONICA MINOLTA spectrophotometer, model CM-2600d under D65 illuminant using a standard 10° observer. The color difference (*ΔE*) of the samples using the base of measurements of the CIE coordinates were calculated based to:

$$\Delta E = \sqrt{(\Delta L^*)^2 + (\Delta a^*)^2 + (\Delta b^*)^2} \quad (2)$$

Where ΔL^* indicates the color luminosity difference between the samples coated with the NPs and the pure cotton fabric, Δb^* yellow/blue coordinate difference and Δa^* coordinate difference between the samples nanocoated with the nanomaterials and control fabric, respectively. Colorimetric data and the reflectance spectra of the coated samples were determined using a diffuse reflectance spectrophotometer (Konica Minolta CM-2600d, USA), employing a D65 light source lamp and a 10° visual angle. In addition, after the coating process, the impregnated samples were analyzed to assess the resistance with which the solution imprinted the color on the fabric, absorbing light in the visible region through *K/S* values calculated from its reflectance measurements using the Kubelka-Munk equation [42]:

$$\frac{K}{S} = \frac{(1-R)^2}{2R} \quad (3)$$

where *K* and *S* are absorption and scattering spectral coefficients, respectively; *R* is the spectral reflectance ratio [43].

2.5. UPF analysis

The UV protection ability under UV light of treated samples was determined according to UPF values estimated by AS/NZS 4399-1996 using SDL Atlas M284 device. Specimens scanning was started and the UV transmittance of the sample from

280 to 400 nm, with logging of transmittance data at least every 1 nm, was carried out in triplicate. Then, UPF values was calculated according to:

$$UPF = \frac{\int_{\lambda_1}^{\lambda_2} E(\lambda).S(\lambda).d\lambda}{\int_{\lambda_1}^{\lambda_2} E(\lambda).S(\lambda).T(\lambda).d\lambda} \quad (4)$$

where E(λ) is the efficiency of the erythemal spectrum, S(λ) is the solar spectral irradiance (W /m^2/nm) and spectral distribution of the radiation, T(λ) is the spectral transmission of the samples, and delta λ is the measured wavelength range (nm). The resulting UPF value was based on the average of the values sought from the twill fabric readings in the weft, warp and diagonal directions (Fig. 1). The evaluations were carried out in the warp, diagonal and weft direction in which the resulting UPF was based on the average of the three directions.

2.6. Assessing durability after washing

Samples impregnated with NPs were estimated to evaluate the UPF durability under UV light after washing cycles. The sample washing process followed the standards established by AATCC 61-2008 2A using the WT-16B wash fastness tester (MATHIS, SP, BR) at 40 °C in the presence of 50 steel balls, where a wash cycle is equivalent to five household washes. Then, the samples were dried at room temperature for UPF evaluation.

3. Results and discussions

3.1. FTIR

The FTIR analyzes were performed both on the final product of the synthesis (N-GQD) and on the used precursors (citric acid and urea), according to Fig. 2. The formation of bands referring to the NH stretch was observed in the region 1319 cm^{-1} in the N-GQD spectrum. The presence of the C-N stretch appears in the urea and N-GQD spectrum at 1562 cm^{-1}. This evidences the integration of nitrogen from the urea of the N-GQD chains in the pyrolysis reaction process. The C=O bond appears in the three spectra analyzed in the 1666 cm^{-1} region. The O-H radical appears in a wide region around 2900 cm^{-1} in citric acid and N-GQD. Characteristic stretches of C-H bonds are observed in the 1447 and 825 cm^{-1} regions of the N-GQD spectrum. The presence of COOH is evidenced in the 1400 cm^{-1} region. The COOH and N-H groups are responsible for causing hydrophilicity and stability in N-GQD in aqueous systems [44–46].

It can be assumed according to Fig. 3 the formation of N-GQD initially involves a dehydration and condensation of citric acid, initiating the formation of a sheet-shaped structure. This intermolecular dehydration reaction occurs mainly between the COOH groups of neighboring citric acid molecules. N atoms are added to the graphene structure through intramolecular dehydration between the amide and the COOH. Nitrogen can be present in the graphene structure in pyrrolic, pyridic or graphitic rings. In addition, a remaining fraction of COOH and ketone can also form in the graphene structure [37,39,47].

3.2. Photoluminescent properties

To explore the optical properties of the synthesized N-GQD, photoluminescence and UV-vis absorption spectra were obtained from the material that was lyophilized and later diluted. Fig. 4 (a) shows the absorbance spectrum of N-GQD in a range

between 300 and 600 nm. The sample has absorption peaks in the regions around 211, 270, 327 nm and extended into the visible region, resulting in a yellowish color. This wide absorption range allows excitation with broad spectrum light sources, from sources with a high UV index (eg sunlight) to low UV index sources (eg some LED lamps). The origin of the 211, 270 and 327 nm peaks arose from the electron transitions from π to π * from C = C, C = N and C = O, respectively, consistent with the literature [48–51]. Thus, the absorption spectrum can also provide fingerprints of the N-GQD structures. These surface states present in N-GQD can result in emissive traps. That is, when a certain excitation wavelength illuminates the N-GQD, a surface state emitting trap will dominate the emission. In general, N-GQD photoluminescence can be attributed to the combination or competition effect between intrinsic state emission and defect state emission. Due to the effect of quantum confinement, the UV-vis photoluminescence spectra of N-GQD can vary according to particle size. Furthermore, the synthesis method, network defects, doping and oxygen ratio are factors that can also influence the absorption and emission behavior of this nanomaterial [52].

It is reported that the band gap caused by quantum confinement effects is size dependent, i.e., the smaller the size, the larger the energy gap. Consequently, the strong quantum confinement effect leads to improved gap opening. When plotting the Tauc graph, which relates the square of the absorption energy (αhv, where α is the absorbance and hv is the photon energy) with the photon energy, the energy of the direct band gap is determined by the tangent line to resulting curve as 3.53 eV [53] (Fig. 4(b)).

In an analysis carried out in a fluorimeter, the excitation radiation was varied between 340 and 470 nm, with an increment of 10 nm, while the emission was monitored in the range between 375 and 650 nm, according to Fig. 4(c). It was observed that the radiations that caused a greater visible photoluminescent effect, that is, when the highest peaks of radiation emission occur in the range of 400 to 700 nm, are found in the UV region of the electromagnetic spectrum, with the excitation peak at 370 nm causing an emission with a peak at 452 nm. Furthermore, as the excitation wavelength is changed from 340 to 470 nm, the resulting emission peak shifts to longer wavelengths and its intensity gradually decreases. These emissions visually correspond to several variations of blue and green tones, as can be seen in the CIE 1931 chromaticity diagram (Fig. 4(d)).

The quantum yield of N-GQD was 25.36%, based on the methodology of Allen [54] and Ishida et al. [55]. This result indicates that the nitrogen doping process from the use of urea in the citric acid carbonization process increases the photoluminescent efficiency of carbon quantum dots, as reported in the literature. Furthermore, the quantum yield of undoped species is also reported to be in the range of 7-11%. Chen et al. [56] also synthesized GQDs derived from citric acid, but without adding urea in the process, and achieved a quantum yield of 9%. As has been reported in the literature, carbon-based luminescent nanomaterials without surface passivation generally have low quantum yields [57].

Also, the photoluminescence intensity of these nanomaterials can also vary according to pH, solvent, average particle size, edge configuration, defects, doping, citric acid carbonization time and temperature, among others [56]. The GQD-N emission mechanism depends on ordered sp^2 clusters with sizes of about 1 nm that are isolated within the sp^3 C-O matrix. The presence of sp^2 molecular clusters located within an sp^3 matrix can lead to confinement of π electrons. Radiative recombination of electron/vacancy pairs in these sp^2 clusters can give rise to fluorescence [58,59].

3.3. XRD

Fig. 5 shows the XRD patterns. It is observed in the image the positions of the main peaks of the N-GQD of the axis (2θ) appear close to the characteristic peak region of graphite (002); although the peak, related to graphite, is more acute than that of N-GQD. This clearly suggests that citric acid carbonization leads to graphite-like structures. However, the absence of sharp peak in the case of the XRD pattern of N-GQD may be related to the disordered structure of N-GQD, due to the presence of large amounts of oxygenated and nitrogen functional groups in its structure, which can cause a considerable lack of order in the graphene quantum dots [60,61]. The crystallite size was estimated at 4.1 nm using the Scherrer equation, this value was similar to the average particle size of 3.0 nm calculated based on the HRTEM N-GQD images.

The TiO_2 powder synthesized via sol-gel was subjected to XRD as shown in Fig. 5(b), so that it had characteristics related to its formation. In relation to the TiO_2 phase, it was possible to perceive well defined peaks, being found between the 20° to 70° regions. The characteristic peaks of TiO_2 in the anatase phase were observed at 2θ = 25.3°; 37.8°; 48.0°; 54.0°; 55.0° and 69.0° in accordance with JCPDS reference sheet 00-002-0387 and study by Behnajady et al. [41], while the brookite phase peaks were observed at 30.1° and 63.1° according to JCPDS 00-029-1360. The diffractogram also allowed the visualization of its crystalline structure, which is consistent with a tetragonal system. The crystallite size was estimated at 8 nm and calculated based on the average of the three most intense and defined peaks (25.25°; 37.80° and 47.97°).

Already in fig. 5(c) All fabric samples (treated or not) showed the presence of peaks 2θ = 15°, 16°, 22° and 34° referring to the crystallographic planes (101), (10$\bar{1}$), (002) and (040) characteristic of cellulose I. Furthermore, all these diffractograms exhibited great similarity, indicating that no polymorphic transformation occurred in the unit cell structure of the cellulose crystals. It is observed that in the samples treated only with N-GQD there was no presence of any peak characteristic of the quantum dot, which is explained by the weak signal of the element as can be seen in its diffractogram

The sample functionalized only with TiO_2 showed peaks at 2θ = 25°; 48º; 54º; 55° referring to the planes (101), (200), (105) and (211) of the anatase phase. The sample treated with N-GQD and TiO_2 did not show characteristic peaks of either component. According to Ou et al. [62], the association between N-GQD and TiO_2 can result in a decrease in the signal intensity characteristic of TiO_2 in an X-ray diffractogram, which is why no signal was observed in the sample in Fig. 5(c) [60].

3.4. HRTEM

The micrographs of the nanostructures performed by the HRTEM technique are shown in Fig. 6. According to Fig. 6(a), it is observed that N-GQD are uniformly dispersed and without agglomeration. Regarding geometry, the particles have a spherical shape, with heterocyclic formation, mean particle size of 3 nm +/- 0.8 nm and presence of lattice fringes with a spacing of 0.21 nm referring to the d100 plane similar to the hexagonal pattern of graphene [63]. These characteristics are similar in studies that used citric acid as a precursor [48-50]. Furthermore, the SAED patterns in Fig. 6. (b) show the semi-crystalline structure of N-GQD synthesized via hydrothermal which corroborates the XRD pattern (Fig. 5 (a)). As shown in Fig. 6(c) the sol-gel synthesis method provides TiO_2 NPs with a mean diameter of 12.8 nm +/- 2.9 nm based on the normal fit (insert Fig. 6(c)). Although the presence of clusters is evident, the HRTEM image of the TiO_2 NPs shows a crystalline structure, as shown by the formation of

concentric rings as a result of diffraction of the crystallographic planes of the SAED analysis (Fig. 6 (d) and by the presence of the lattice fringes with a spacing of 0.35 nm corresponding to the d101 plane value of the TiO_2 anatase [53] in the HRTEM (insert Fig. 6 (c)).

Already in Fig. 6 (e), the presence of TiO_2 NPs decorated with N-GQD as highlighted in the image is observed. From Fig. 6 (f)), the SAED pattern shows concentric and more noticeable rings than the SAED pattern of isolated N-GQD, which corroborates the presence of TiO_2 by its crystallographic planes of the material in the semi-crystalline structure of the quantum dots, which demonstrates that the nanocoating process via hydrothermal resulted in the junction between organic/inorganic nanomaterials.

3.5. Characterization of cotton fabric nanocoated

3.5.1. XPS

The surface chemical composition of the pristine CO, PC and nanocoated samples were also analyzed by XPS. Fig. 7 (a) showed the deconvoluated C1S curve of XPS of the pristine CO fabric where it displays three peaks that correspond to the carbon signal in the connections. The peaks at 284.9, 286.7 and 288.1 eV corresponds to C-C / C-H, C-O-H and C-O-C cellulose bonds, respectively [64]. Both the C1S curve and the N1s curve of the analyzes were evaluated and the characteristic peaks of the chemical composition of PnGC and PnGC1 are shown in Fig. 7 (b) where the deconvoluated C1s spectrum clearly shows four peaks in 284.5, 285.8, 287.5 and 288.6 eV attributed sp^2-sp^2 C (C - C), N- sp^2 C (C - N), CO/C-OH, and O-C = O binding, respectively. It is also observed that in the deconvoluated N1s XPS spectrum (insert Fig.7 (b)) comprised three peaks with connection energies at 399.1, 400 and 400.8 eV corresponding to the presence of nitrogen in the pyridine, pyrrolic and grafitic ring, present in the chemical structure N-GQD [64,65].

With the XPS spectra obtained in Fig. 7 (c) it was possible to identify the presence of TiO_2 NPs on cotton (PTC sample). According to the literature, a characteristic XPS spectrum of TiO_2, which corresponds to the Ti^{+4} oxidation state, has two lines, one corresponding to photoelectrons emitted by the Ti 2p level and another to the photoelectrons of the oxygen 1s level. With the high electronegativity of oxygen, Ti loses more electrons as the number of oxygen atoms around it increases, and therefore the binding energy of the 2p core level electrons shifts to higher energies. Due to the spin-orbit interaction, the 2p level of Ti separates into the $2p_{3/2}$ levels, which corresponds to the most intense line in the XPS spectrum, and into the $2p_{1/2}$. The 2p doublet line intensities ratio is 2:1 and the energy separation is approximately 5.7 eV. Both the 458.60 and 464.3 eV power lines are deconvoluted to two peaks, which correspond to Ti^{+4} $2p_{3/2}$ and Ti^{+4} $2p_{1/2}$ respectively [66]. The O1s peak (insert Fig. 7(c)) represents the oxygen deconvolution data where in the power line 530 eV corresponds to the O1s peak at the position of the Ti-O peak. The peak area corresponding to the hydroxyl group (OH) in the energy line of energy 531.31 eV belongs to adsorbed water as shown in Fig. 7(c) [67].

In Fig. 7(d) we have spectral data obtained via XPS. The spectrum corresponds to the PTC and their respective intensities, as well as the PTnGC. It was necessary to make this comparison to identify the presence of nitrogen in the N-GQD molecule. It is noticed the presence of the N1s peak related to the presence of N-GQD and its respective deconvolution of the high resolution XPS peak spectrum of N1s at 400 eV, a difference is noticed when compared to deconvoluted nitrogen in Fig. 7(d). The presence of noise in this spectrum is due to the low intensity obtained from nitrogen,

caused by the presence of TiO_2 which tends to reduce the crystallinity of N-GQD as seen in Fig. 6 (b) of HRTEM/SAED results. However, the spectrum reveals the existence of pyridine N (399.7 eV), pyrrolytic N (400.3 eV) and graphitic N (401.5 eV), proving the existence of N-GQD in the respective PVA/TiO_2/N-GQD nanocoatings [68].

3.5.2. Colorimetric properties

The colorimetric coordinate was evaluated by Eq.(2) and colour strength data corresponding to Fig. 8 were obtained using Kubelka-Munk Eq.(3). It was observed that under the conditions of a D65 illuminant, the treated samples did not obtain discrepant *K/S* intensities in relation to the pristine CO, indicating that the hydrothermal nanocoating process did not change the color luminosity of the cotton fabric, however, the negative ΔL (table insert Fig. 8 (a)) value for all treated samples indicates a darkening of the functionalized fabrics. Due to the absorption sites present in the quantum dots as C=C, C=O and C=N, evidenced by the FTIR and XPS, the samples that had the largest negative deviations of *ΔL* (taking into account a color tolerance = 1) were in order those treated with N-GQD with greater concentration (PnGC1), N-GQD (PnGC) and N-GQD/TiO_2 (PTnGC). This pattern is also related to the intensity variations of *K/S* curves. With all these changes in L*a*b coordinates caused by treatments on the fabric, there was a significant change in its ΔE values, indicating that the presence of N-GQD and TiO_2 NPs promoted changes in the color of pristine CO, such as shows the images of samples (Fig. 8 (b)). Thus, it is possible to observe that the PnGC1, PnGC and PTnGC had a considerable color shift to red and yellow compared to the untreated fabric. While the sample treated only with the binder and the one treated with TiO_2 had a more considerable shift towards yellow.

With all these changes in the *L*a*b* coordinates caused by the treatments on the fabric, there was a considerable change in the *ΔE* values, indicating that the color changes caused by N-GQD in the fabrics were high. It is noticed that the PnGC1presented a dark brown color (*ΔE* = 50.79). Thus, N-GQD can cause remarkable color changes according to the concentration applied in the treatment, and can even replace a finishing process. It was observed that PC (*ΔE* = 2.10) and PTC (*ΔE* = 4.81) also had reasonable color changes.

A high whiteness is important for many dyeing or printing processes. However, a significant reduction of these factors was observed for PnGC, PnGC1 or PTnGC, logically due to the formation of color on cotton fabric. This indicates that when a high degree of whiteness is needed, excessive use of N-GQD should be avoided or used in conjunction with other methodologies to increase the whiteness degree on fabric. Furthermore, Fig. 8 (b) represents images colors of fabric samples nanocoated in the presence of natural light and in the presence of UV light. It is possible to notice the luminescent effect in all samples treated with N-GQD, evidenced by the lighter tone in the images.

3.5.3. FE-SEM

The FE-SEM micrographs of nanoparticle treated and untreated samples are shown in Fig. 9. As shown in Fig. 9 (a), the control fabric is characterized by their longitudinal section with a flat ribbon shape, with a smooth appearance and convolutions that show the fibrillar structure of the cotton fibers. Unlike untreated samples, the micrographs in Fig. 9 (b – c) exhibit a rougher and more wrinkled surface for the PnGC and PTnGC samples, respectively, clearly indicating the process of coating the NPs with the PVA as it is a polymeric material with a high film-forming capacity [69], which results in a thin coating of PVA molecules. However, N-GQD and

TiO_2 NPs is not easily observed under high magnification. Therefore, the deposition of the N-GQD/TiO_2 on the surface of the cotton fabric was confirmed by the images of the rough surface of fabric.

3.5.4. AFM

Fig. 10 corresponds to the 2D AFM micrographs obtained on the surface of the cotton fibers before and after the nanocoating process. Fig. 10 (a) presents the fiber topology of the fabric absent of NPs, which observes the morphological characteristics of the surface of cotton fibers with the presence of nanofibrils, valleys and ridges, also previously visualized in the FEG-SEM micrographs. Furthermore, the 3D image of the center of Fig. 10 (a) shows the depth of the valleys. This morphology is responsible for the variation in the surface roughness of the cotton fiber and, consequently, influencing the maximum roughness values obtained (48.32 nm). Therefore, the cotton fiber presented an average roughness (*Ra*) = 12.3 nm. After the PVA/N-GQD immobilization process on the fabric (Fig. 10 (b)), the image shows the presence of shallower crevices and valleys, with greater roughness due to the presence of the quantum dot clusters with certain clusters of NPs that promoted a decrease in roughness on the fiber surface, with *Ra* = 7.26 nm, as shown by the line profile. However, the presence of TiO_2 on the PTnGC (Fig. 10 (c)) caused an increase in the maximum fabric surface roughness equal to 39.36 nm which contributed to a significant increase in *Ra* = 16.5 nm higher than the *Ra* of the PnGC and lower than the control sample. Smaller particles manage to accommodate themselves within the valleys and the larger ones stay on the fiber surface, as observed in the same sample submitted to FE-SEM analysis. That can be caused by the presence of TiO_2, as it is noticed an average variation of NPs sizes.

3.5.5. UV protection

The samples containing TiO_2, N-GQD and PVA as well as the cotton fabric without nanocoating were evaluated for their UV protection property, according to the results presented regarding the tests performed on the fabric in the warp direction (Table 1), diagonal (Table 2) and plot (Table 3), and in Fig. 11, representing the mean of the UPF values of the respective analyses. All other samples coated with NPs were responsible for the decrease in transmittance in the range between 280 and 400 nm in the electromagnetic spectrum. The UPF is commonly used due to the consideration of its calculation in erythemal spectral efficacy and irradiance at a given wavelength. Therefore, it could also be defined as the ratio between the potential erythema effect and the actual erythema effect transmitted by the fabric by radiation [70]. It was observed that the untreated cotton fabric had a UPF 11 (warp), 12 (diagonal), 13 (weft) and an average of 12, considered insufficient to protect human skin from UV radiation from the sun or artificial sources such as lamps or welding processes. But it is known that cotton, linen, acetate and rayon fabrics offer low protection against UV radiation when not functionalized with some anti-UV agent properly [71].

The fabric modified only with the binding agent PVA also presented a result characterized as insufficient according to the standard, a UPF value of +10 both in the weft (13), diagonal (14) and warp (14) direction. Thus, the cotton fabric functionalized with N-GQD was responsible for an increase in the UPF to 31, classified as very good according to the adopted standard. And when you increase the concentration of N-GQD to 10 times, more in the fabric functionalization process, you get an increase in the UPF to +50, classified as excellent. The functionalization of the cotton fabric with

TiO_2 presented an excellent result of UV protection in the warp (334), diagonal (431), weft (505) direction and an average of 423 or +50. But, due to its limited application in textiles for UV protection due to the requirements of the International Agency for Research on Cancer - IARC, as described by Baan [25], the synergy between N-GQD of lower concentration (0.1 g/L) with TiO_2 was evaluated. And the result was a UPF in the warp direction of 93, diagonal 103, weft of 137 and an average of 111 or +50, according to tables 2-4 and Fig. 11 below, which characterizes the functionalization performed with N-GQD/TiO_2 was responsible for an increase in the UPF to 111 ("excellent").

Table 2 - UPF - AU/NZS 4399 (warp)

Sample	UVA	UVB	Blocked UVA (%)	Blocked UVB (%)	UVR	UPF	Classification
Pristine CO	12.39	7.45	87.61	92.55	88.75	11	low protection
PC	10.71	6.64	89.29	93.36	90.23	13	low protection
PTC	1.94	0.18	98.06	99.82	98.44	334[a]	excellent
PnGC	4.07	2.87	95.93	97.13	96.21	32	very good
PnGC1	0.38	0.32	99.62	99.68	99.63	303[a]	excellent
PTnGC	2.04	0.95	97.96	99.05	98.20	93[a]	excellent

[a]UPF +50

Table 3 - UPF - AU/NZS 4399 (Diagonal)

Sample	UVA	UVB	Blocked UVA (%)	Blocked UVB (%)	UVR	UPF	Classification
Pristine CO	12.00	7.04	88.00	92.96	89.14	12	low protection
PC	10.40	6.49	89.60	93.51	90.50	14	low protection
PTC	1.65	0.14	98.40	99.82	98.71	431[a]	excellent
PnGC	4.05	2.87	95.95	97.13	96.22	31	very good
PnGC1	0.41	0.35	99.59	99.65	99.60	284[a]	excellent
PTnGC	2.04	0.91	97.96	99.09	98.21	103[a]	excellent

[a]UPF +50

Table 4 - UPF - AU/NZS 4399 (weft)

Sample	UVA	UVB	Blocked UVA (%)	Blocked UVB(%)	UVR	UPF	Classification
Pristine CO	11.71	6.78	88.29	93.22	89.42	13	low protection
PC	10.31	6.19	89.69	93.81	90.64	14	low protection
PTC	1.51	0.11	98.49	99.90	98.80	505[a]	excellent
PnGC	4.38	3.13	95.62	96.87	95.91	29	very good
PnGC1	0.37	0.31	99.63	99.69	99.64	334[a]	excellent
PTnGC	1.48	0.66	98.52	99.34	98.70	137[a]	excellent

[a]UPF +50

3.5.6. Durability of UV protection

It is possible to observe that the functionalization of cotton fabric with N-GQD has an excellent protection efficiency in the UVA region, while the treatment with TiO_2 has a excellent protection efficiency in the UVB region. In addition to the transmittance spectra obtained, UPF values were obtained in order to evaluate the UV protection

capacity of cotton fabrics according to the values presented in Table 4, which shows UPF values for washed and unwashed samples.

As shown in Fig. 12(b), it was verified that the control fabric had UPF 12 before and after 20 washing cycles, classified according to the standard as insufficient to protect human skin from UV radiation. Differently, the PnGC sample obtained UPF 31 classified as "very good" according to the adopted standard and a slight reduction of the UPF value to 25, showing that although some N-GQD suffered desorption, the sample obtained a good UV protection after the washing process. For the PnGC and PTnGC samples there was an increase in the UPF to +50, showing that all these treatments presented a classification considered excellent for UV protection in textiles. Therefore, it can be seen that both materials are good UV absorbers and their UPF values remained unchanged after the washing process, indicating that the coating with NPs provides the cotton fabric with satisfactory properties for applications involving UV protection and durability of the treatment after successive washes.

The UV absorption properties of TiO_2 occur due to its semiconductor behavior. When TiO_2 is illuminated by radiation with energy greater than its bang gap, the electrons absorb the photon energy and are excited to cross the band gap to produce the pairs of electrons and holes [72]. The UV absorption properties of N-GQD occur due to the presence of the π–π* transitions (230-250 nm) of the C=C aromatic bonds and the n–π* transition of the C=O or C=N bonds (327 nm), as seen in absorbance spectroscopy.

4. Conclusion

Fabric functionalized with TiO_2 and Nitrogen doped graphene quantum dots (N-GQD) NPs in a hydrothermal process using Polyvinyl alcohol (PVA) as a binding agent promoted a material that protect against ultraviolet (UV) radiation. Uncoated fabrics showed no protection while fabrics loaded with nanocoating resulted in high ultraviolet protection factor (UPF) values even after the washing process, indicating that in addition to the anti-UV capacity the material has a N-GQD and N-GQD/TiO_2 nanocoating on cotton fabric that is durable to domestic washing cycles. Thus, the way in which the fabrics were loaded with nanoparticles can be easily applied to existing machinery allows a high-efficiency material to be practically reproduced in industry.

5. References

[1] Wright F, Weller RB. Risks and benefits of UV radiation in older people: More of a friend than a foe? Maturitas 2015;81:425–31.

[2] Wang SQ, Balagula Y, Osterwalder U. Photoprotection: a review of the current and future technologies. Dermatologic Therapy 2010;23:31–47.

[3] Ben Salah M, Hallé S, Tuduri L. Efficiency of five chemical protective clothing materials against nano and submicron aerosols when submitted to mechanical deformations. Journal of Occupational and Environmental Hygiene 2016;13:425–33.

[4] Lautenschlager S, Wulf HC, Pittelkow MR. Photoprotection. The Lancet 2007;370:528–37.

[5] Khan A, Nazir A, Rehman A, Naveed M, Ashraf M, Iqbal K, et al. A review of UV radiation protection on humans by textiles and clothing. International Journal of Clothing Science and Technology 2020.

[6] de Dio Ferreira D, Galvao TD, Appoloni CR. Total Reflection X-ray Fluorescence spectrometry determination of titanium dioxide released from UV-protective textiles during wash. Applied Radiation and Isotopes 2020;165:109345.

[7] Georgescu SR, Mitran MI, Mitran CI, Matei C, Caruntu A, Scheau C, et al. Current Perspectives on the Role of Matrix Metalloproteinases in the Pathogenesis of Basal Cell Carcinoma. Biomolecules 2021;11:903.

[8] Ryšavá A, Vostálová J, Rajnochova Svobodova A. Effect of ultraviolet radiation on the Nrf2 signaling pathway in skin cells. International Journal of Radiation Biology 2021;97:1383–403.

[9] American Cancer Society. Cancer facts & figures 2019. American Cancer Society 2019. https://www.cancer.org/research/cancer-facts-statistics/all-cancer-facts-figures/cancer-facts-figures-2019.html.

[10] Sung H, Ferlay J, Siegel RL, Laversanne M, Soerjomataram I, Jemal A, et al. Global cancer statistics 2020: GLOBOCAN estimates of incidence and mortality worldwide for 36 cancers in 185 countries. CA: A Cancer Journal for Clinicians 2021;71:209–49.

[11] Bauer S. Photoprotection by workwear: ultraviolet protection factors for artificial radiation from welding arcs. Photochemistry and Photobiology 2020;96:917–25.

[12] Kabir SMM, Dhar AK, Koh J. The Influence of a Natural UV Absorber (Areca catechu) on the UV Protection and Antimicrobial Properties of Silk and Nylon Fabrics. Fibers and Polymers 2021;22:382–6.

[13] Mondal S. Nanomaterials for UV protective textiles. Journal of Industrial Textiles 2021:1528083721988949.

[14] Yildirim K, Kanber A, Karahan M, Karahan N. The solar properties of fabrics produced using different weft yarns. Textile Research Journal 2018;88:1543–58.

[15] Román LE, Huachani J, Uribe C, Solís JL, Gómez MM, Costa S, et al. Blocking erythemally weighted UV radiation using cotton fabrics functionalized with ZnO nanoparticles in situ. Applied Surface Science 2019;469:204–12.

[16] Kocić A, Bizjak M, Popović D, Poparić GB, Stanković SB. UV protection afforded by textile fabrics made of natural and regenerated cellulose fibres. Journal of Cleaner Production 2019;228:1229–37.

[17] Nascimento JHO, Felipe BHS, Cabral RLB, Ahmad A, da Silva AB, Neto NFA, et al. New Advances of the Nanotechnology in Textile Engineering: Functional Finishing with Quantum Dots and Others Nanoparticles. Nanomaterials and Nanotechnology: Biomedical, Environmental, and Industrial Applications 2021:239.

[18] Afroj S, Karim N, Wang Z, Tan S, He P, Holwill M, et al. Engineering graphene flakes for wearable textile sensors via highly scalable and ultrafast yarn dyeing technique. Acs Nano 2019;13:3847–57.

[19] Carneiro JO, Teixeira V, Nascimento JHO do, Neves J, Tavares PB. Photocatalytic activity and UV-protection of TiO2 nanocoatings on poly (lactic acid) fibres deposited by pulsed magnetron sputtering. Journal of Nanoscience and Nanotechnology 2011;11:8979–85.

[20] Rashid MM, Simončič B, Tomšič B. Recent advances in TiO2-functionalized textile surfaces. Surfaces and Interfaces 2021;22:100890.

[21] Yang M, Liu W, Jiang C, Xie Y, Shi H, Zhang F, et al. Facile construction of robust superhydrophobic cotton textiles for effective UV protection, self-cleaning and oil-water separation. Colloids and Surfaces A: Physicochemical and Engineering Aspects 2019;570:172–81. https://doi.org/10.1016/J.COLSURFA.2019.03.024.

[22] Bouazizi N, Abed A, Giraud S, El Achari A, Campagne C, Morshed MN, et al. Development of new composite fibers with excellent UV radiation protection. Physica E: Low-Dimensional Systems and Nanostructures 2020;118:113905.

[23] Biswas MC, Islam MT, Nandy PK, Hossain MM. Graphene Quantum Dots (GQDs) for Bioimaging and Drug Delivery Applications: A Review. ACS Materials Letters 2021;3:889–911.

[24] Bressi V, Ferlazzo A, Iannazzo D, Espro C. Graphene Quantum Dots by Eco-Friendly Green Synthesis for Electrochemical Sensing: Recent Advances and Future Perspectives. Nanomaterials 2021;11:1120.

[25] Baan RA. Carcinogenic hazards from inhaled carbon black, titanium dioxide, and talc not containing asbestos or asbestiform fibers: recent evaluations by an IARC Monographs Working Group. Inhalation Toxicology 2007;19:213–28.

[26] Kale RD, Potdar T, Kane P, Singh R. Nanocomposite polyester fabric based on graphene/titanium dioxide for conducting and UV protection functionality. Graphene Technology 2018;3:35–46.

[27] Stan MS, Nica IC, Popa M, Chifiriuc MC, Iordache O, Dumitrescu I, et al. Reduced graphene oxide/TiO2 nanocomposites coating of cotton fabrics with antibacterial and self-cleaning properties. Journal of Industrial Textiles 2019;49:277–93.

[28] Stan MS, Badea MA, Pircalabioru GG, Chifiriuc MC, Diamandescu L, Dumitrescu I, et al. Designing cotton fibers impregnated with photocatalytic graphene oxide/Fe, N-doped TiO2 particles as prospective industrial self-cleaning and biocompatible textiles. Materials Science and Engineering: C 2019;94:318–32.

[29] Cao X, Pan X, Couvillion SP, Zhang T, Tamez C, Bramer LM, et al. Fate, cytotoxicity and cellular metabolomic impact of ingested nanoscale carbon dots using simulated digestion and a triculture small intestinal epithelial model. NanoImpact 2021;23:100349.

[30] Hai X, Feng J, Chen X, Wang J. Tuning the optical properties of graphene quantum dots for biosensing and bioimaging. Journal of Materials Chemistry B 2018;6:3219–34.

[31] Sun H, Gao N, Dong K, Ren J, Qu X. Graphene Quantum Dots-Band-Aids Used for Wound Disinfection. ACS Nano 2014;8:6202–10. https://doi.org/10.1021/nn501640q.

[32] Wongrerkdee S, Pimpang P. Ultraviolet-shielding and water resistance properties of graphene quantum dots/polyvinyl alcohol composite-based film. Journal of Metals, Materials and Minerals 2020;30:90–6.

[33] Emam HE, El-Shahat M, Hasanin MS, Ahmed HB. Potential military cotton textiles composed of carbon quantum dots clustered from 4–(2, 4–dichlorophenyl)–6–oxo–2–thioxohexahydropyrimidine–5–carbonitrile. Cellulose 2021;28:9991–10011.

[34] Shareena TPD, McShan D, Dasmahapatra AK, Tchounwou PB. A review on graphene-based nanomaterials in biomedical applications and risks in environment and health. Nano-Micro Letters 2018;10:1–34.

[35] Omar WIW, Soon CF, Ahmad MK, Shimomura M. Hydrothermal synthesis of biocompatible nitrogen doped graphene quantum dots. Energy & Environment 2021:0958305X20984112.

[36] Zuo D, Liang N, Xu J, Chen D, Zhang H. UV protection from cotton fabrics finished with boron and nitrogen co-doped carbon dots. Cellulose 2019;26:4205–12. https://doi.org/10.1007/s10570-019-02365-5.

[37] Zhu Y, Yan L, Xu M, Li Y, Song X, Yin L. Difference between ammonia and urea on nitrogen doping of graphene quantum dots. Colloids and Surfaces A: Physicochemical and Engineering Aspects 2021;610:125703.

[38] Yu Y, Wang J, Wang J, Li J, Zhu Y, Li X, et al. Highly fluorescent cotton fiber based on luminescent carbon nanoparticles via a two-step hydrothermal synthesis method. Cellulose 2017;24:1669–77.

[39] Ogi T, Iwasaki H, Aishima K, Iskandar F, Wang W-N, Takimiya K, et al. Transient nature of graphene quantum dot formation via a hydrothermal reaction. Rsc Advances 2014;4:55709–15.

[40] Dong Y, Shao J, Chen C, Li H, Wang R, Chi Y, et al. Blue luminescent graphene quantum dots and graphene oxide prepared by tuning the carbonization degree of citric acid. Carbon 2012;50:4738–43.

[41] Behnajady MA, Eskandarloo H, Modirshahla N, Shokri M. Investigation of the effect of sol–gel synthesis variables on structural and photocatalytic properties of TiO2 nanoparticles. Desalination 2011;278:10–7.

[42] Tang AYL, Lee CH, Wang YM, Kan CW. A study of PEG-based reverse micellar dyeing of cotton fabric: reactive dyes with different reactive groups. Cellulose 2019;26:4159–73. https://doi.org/10.1007/s10570-019-02340-0.

[43] Ahmad I, Kan C. Visible-Light-Driven, Dye-Sensitized TiO2 Photo-Catalyst for Self-Cleaning Cotton Fabrics. Coatings 2017;7:192. https://doi.org/10.3390/coatings7110192.

[44] Zhang P, Zhao X, Ji Y, Ouyang Z, Wen X, Li J, et al. Electrospinning graphene quantum dots into a nanofibrous membrane for dual-purpose fluorescent and electrochemical biosensors. Journal of Materials Chemistry B 2015;3:2487–96.

[45] Xie H, Hou C, Wang H, Zhang Q, Li Y. S, N co-doped graphene quantum dot/TiO 2 composites for efficient photocatalytic hydrogen generation. Nanoscale Research Letters 2017;12:1–8.

[46] Miah M, Bhattacharya S, Gupta A, Saha SK. Origin of high storage capacity in N-doped graphene quantum dots. Electrochimica Acta 2016;222:709–16.

[47] Qu D, Zheng M, Zhang L, Zhao H, Xie Z, Jing X, et al. Formation mechanism and optimization of highly luminescent N-doped graphene quantum dots. Scientific Reports 2014;4:1–11.

[48] Sun X, Li H-J, Ou N, Lyu B, Gui B, Tian S, et al. Visible-Light Driven TiO2 Photocatalyst Coated with Graphene Quantum Dots of Tunable Nitrogen Doping. Molecules 2019;24:344. https://doi.org/10.3390/molecules24020344.

[49] Ke C-C, Yang Y-C, Tseng W-L. Synthesis of Blue-, Green-, Yellow-, and Red-Emitting Graphene-Quantum-Dot-Based Nanomaterials with Excitation-Independent Emission. Particle & Particle Systems Characterization 2016;33:132–9. https://doi.org/10.1002/ppsc.201500196.

[50] Zhu S, Song Y, Zhao X, Shao J, Zhang J, Yang B. The photoluminescence mechanism in carbon dots (graphene quantum dots, carbon nanodots, and polymer dots): current state and future perspective. Nano Research 2015;8:355–81.

[51] Chen Y, Zheng B, Li P, Qi F, Liu J, Zhang W, et al. Ultrafast ammonia-driven, microwave-assisted synthesis of nitrogen-doped graphene quantum dots and their optical properties. Nanophotonics 2017;6:259–67. https://doi.org/10.1515/nanoph-2016-0102.

[52] Li L, Wu G, Yang G, Peng J, Zhao J, Zhu J-J. Focusing on luminescent graphene quantum dots: current status and future perspectives. Nanoscale 2013;5:4015–39.

[53] Ngamta S, Boonprakob N, Wetchakun N, Ounnunkad K, Phanichphant S, Inceesungvorn B. A facile synthesis of nanocrystalline anatase TiO2 from TiOSO4 aqueous solution. Materials Letters 2013;105:76–9.

[54] Allen M. Measurement of Fluorescence Quantum Yields. Thermo Fisher Scientific 2010.

[55] Ishida H, Bünzl J-C, Beeby A. Guidelines for Measurement of Luminescence Spectra and Quantum Yields of Inorganic and Organometallic Compounds in

Solution and Solid State (IUPAC Technical Report). Pure Appl Chem 2016;88(7):701–11.

[56] Chen Y, Jingwei D, Congqiang S, Hao C, Ruixue L, Yuwu W, et al. Blue luminescent graphene quantum dots and graphene oxide prepared by tuning the carbonization degree of citric acid. Carbon 2012;50:4738–43. https://doi.org/10.1016/J.CARBON.2012.06.002.

[57] Li L, Wu G, Yang G, Peng J, Zhao J, Zhu J-J. Focusing on luminescent graphene quantum dots: current status and future perspectives. Nanoscale 2013;5:4015. https://doi.org/10.1039/c3nr33849e.

[58] Ogi T, Iwasaki H, Aishima K, Iskandar F, Wang W-N, Takimiya K, et al. Transient nature of graphene quantum dot formation via a hydrothermal reaction. Rsc Advances 2014;4:55709–15.

[59] Loh KP, Bao Q, Eda G, Chhowalla M. Graphene oxide as a chemically tunable platform for optical applications. Nature Chemistry 2010;2:1015–24.

[60] Raghavan A, Sarkar S, Nagappagari LR, Bojja S, MuthukondaVenkatakrishnan S, Ghosh S. Decoration of graphene quantum dots on TiO2 nanostructures: Photosensitizer and cocatalyst role for enhanced hydrogen generation. Industrial & Engineering Chemistry Research 2020;59:13060–8.

[61] Wu ZL, Gao MX, Wang TT, Wan XY, Zheng LL, Huang CZ. A general quantitative pH sensor developed with dicyandiamide N-doped high quantum yield graphene quantum dots. Nanoscale 2014;6:3868–74.

[62] Ou N-Q, Li H-J, Lyu B-W, Gui B-J, Sun X, Qian D-J, et al. Facet-dependent interfacial charge transfer in TiO2/nitrogen-doped graphene quantum dots heterojunctions for visible-light driven photocatalysis. Catalysts 2019;9:345.

[63] Jin SH, Kim DH, Jun GH, Hong SH, Jeon S. Tuning the photoluminescence of graphene quantum dots through the charge transfer effect of functional groups. ACS Nano 2013;7:1239–45.

[64] Wang J, Lu C, Chen T, Hu L, Du Y, Yao Y, et al. Simply synthesized nitrogen-doped graphene quantum dot (NGQD)-modified electrode for the ultrasensitive photoelectrochemical detection of dopamine. Nanophotonics 2020;9:3831–9.

[65] Jin L, Wang Y, Yan F, Zhang J, Zhong F. The Synthesis and Application of Nitrogen-Doped Graphene Quantum Dots on Brilliant Blue Detection. Journal of Nanomaterials 2019;2019.

[66] Xiong J, Das SN, Kim S, Lim J, Choi H, Myoung J-M. Photo-induced hydrophilic properties of reactive RF magnetron sputtered TiO2 thin films. Surface and Coatings Technology 2010;204:3436–42.

[67] Gouttebaron R, Cornelissen D, Snyders R, Dauchot JP, Wautelet M, Hecq M. XPS study of TiOx thin films prepared by dc magnetron sputtering in Ar–O2 gas mixtures. Surface and Interface Analysis: An International Journal Devoted to the Development and Application of Techniques for the Analysis of Surfaces, Interfaces and Thin Films 2000;30:527–30.

[68] Murali G, Reddeppa M, Seshendra Reddy C, Park S, Chandrakalavathi T, Kim M-D, et al. Enhancing the Charge Carrier Separation and Transport via Nitrogen-Doped Graphene Quantum Dot-TiO2 Nanoplate Hybrid Structure for an Efficient NO Gas Sensor. ACS Applied Materials & Interfaces 2020;12:13428–36.

[69] Pandey S, Pandey SK, Parashar V, Mehrotra GK, Pandey AC. Ag/PVA nanocomposites: optical and thermal dimensions. Journal of Materials Chemistry 2011;21:17154–9.

[70] Wang Q, Hauser PJ. Developing a novel UV protection process for cotton based on layer-by-layer self-assembly. Carbohydrate Polymers 2010;81:491–6.

[71] Sarkar AK. An evaluation of UV protection imparted by cotton fabrics dyed with natural colorants. BMC Dermatology 2004;4:1–8.

[72] Yang H, Zhu S, Pan N. Studying the mechanisms of titanium dioxide as ultraviolet-blocking additive for films and fabrics by an improved scheme. Journal of Applied Polymer Science 2004;92:3201–10.

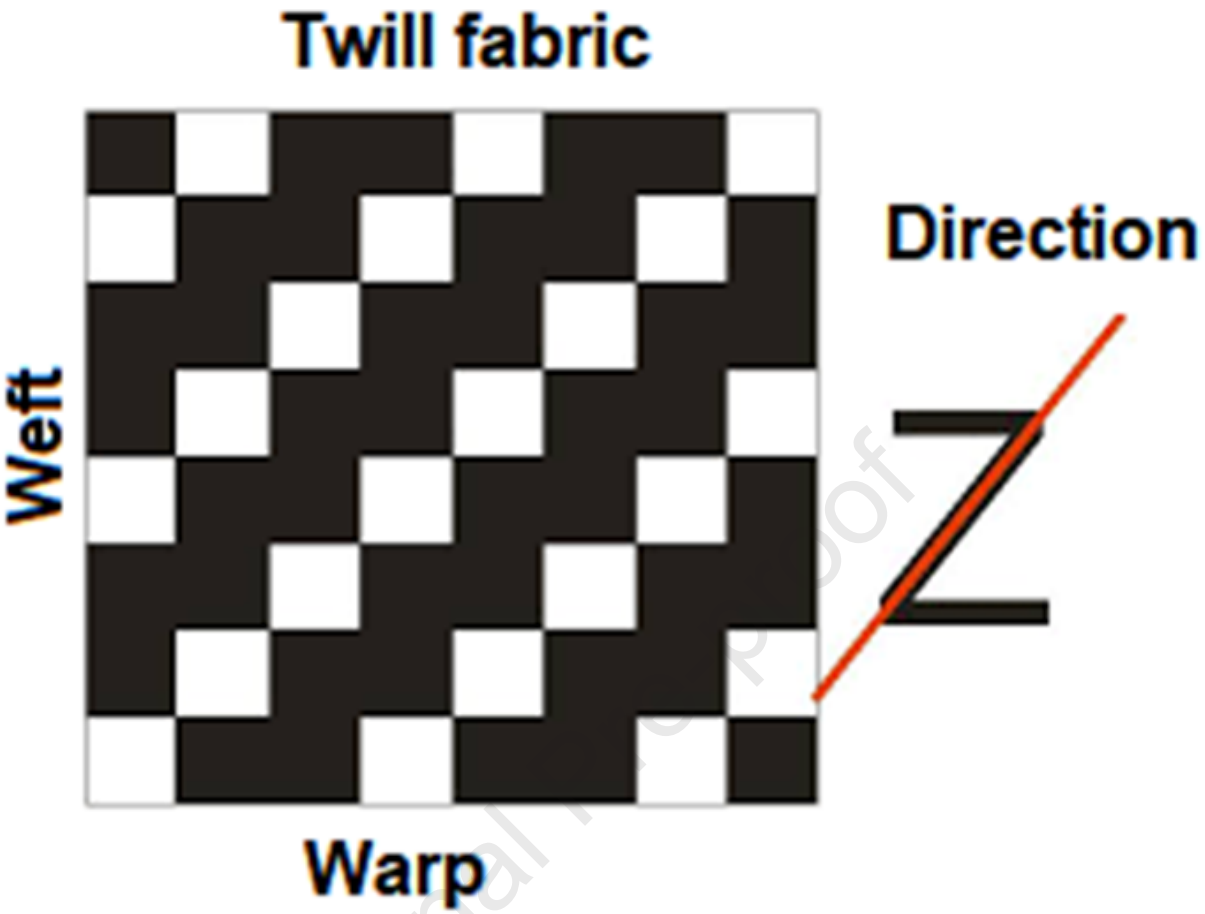

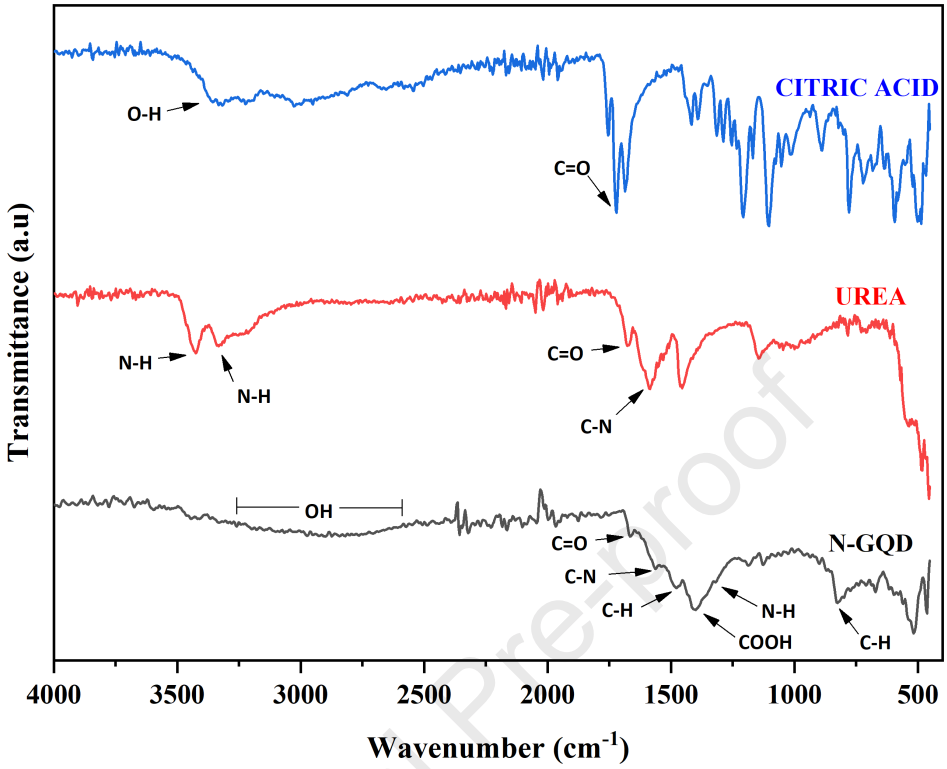

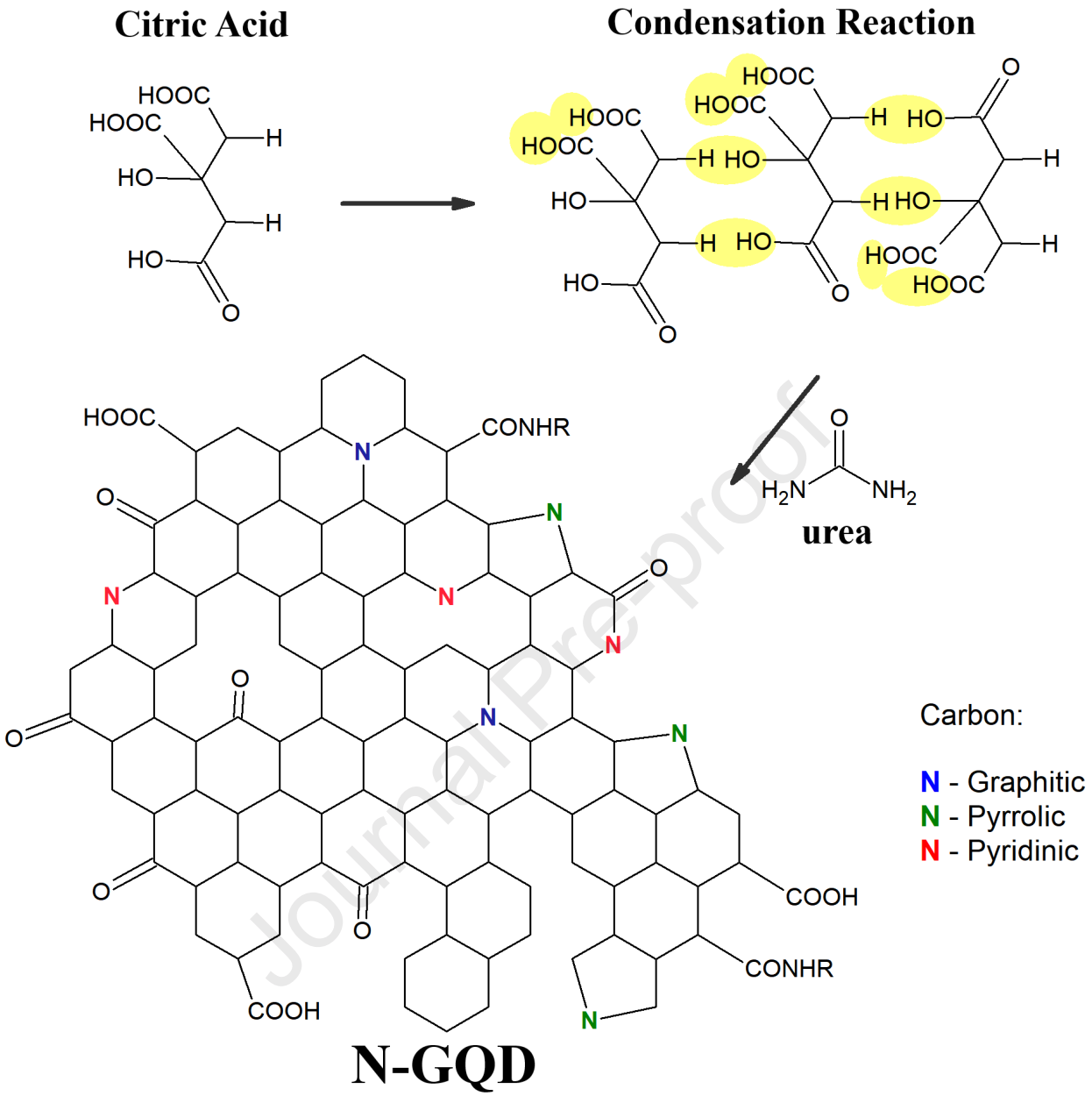

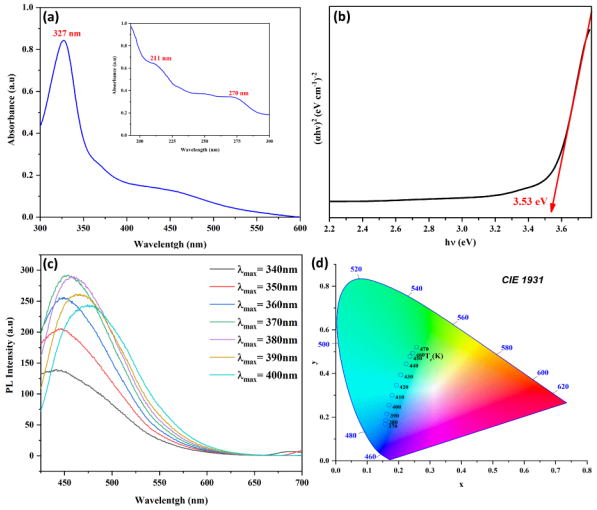

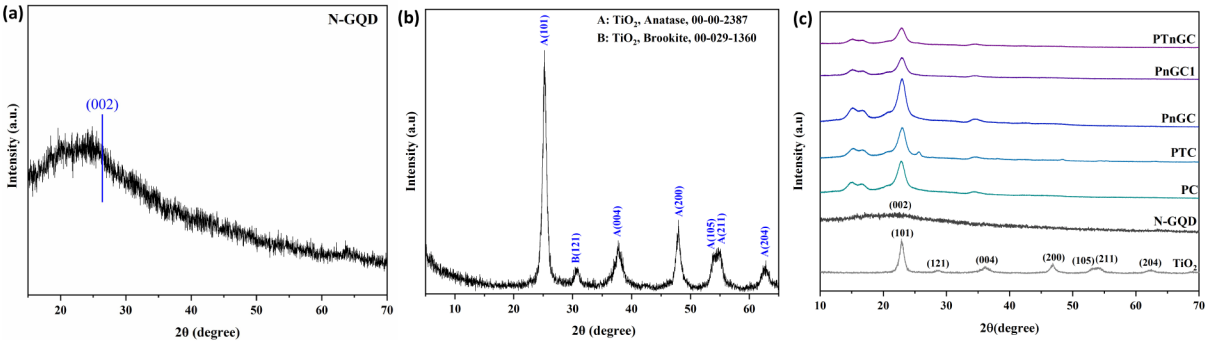

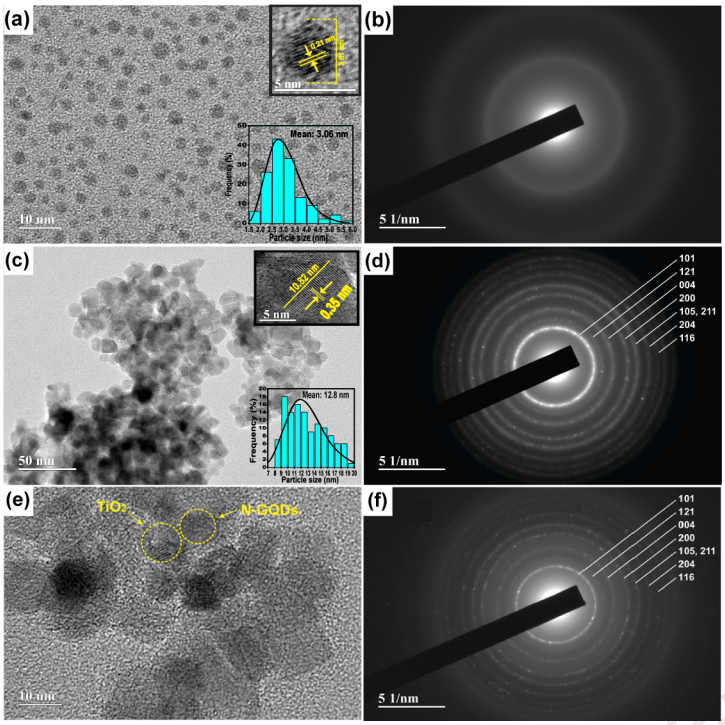

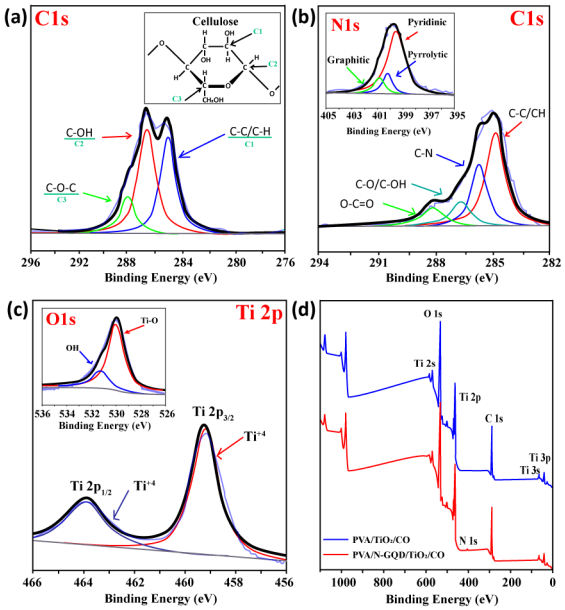

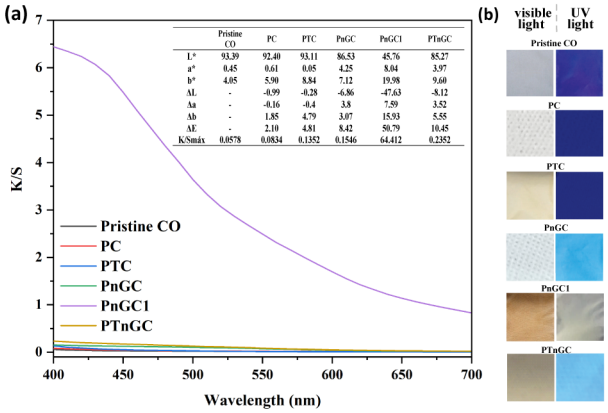

	Pristine CO	PC	PTC	PnGC	PnGCl	PTnGC
L*	93.39	92.40	93.11	86.53	45.76	85.27
a*	0.45	0.61	0.05	4.25	8.04	3.97
b*	4.05	5.90	8.84	7.12	19.98	9.60
ΔL	-	-0.99	-0.28	-6.86	-47.63	-8.12
Δa	-	-0.16	-0.4	3.8	7.59	3.52
Δb	-	1.85	4.79	3.07	15.93	5.55
ΔE	-	2.10	4.81	8.42	50.79	10.45
K/Smax	0.0578	0.0834	0.1352	0.1546	64.412	0.2352

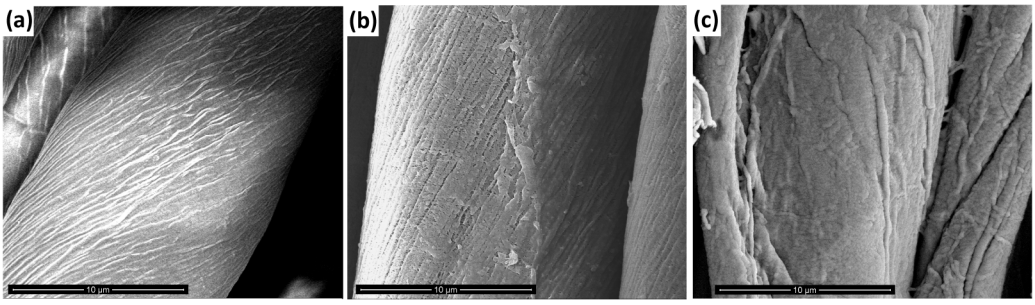

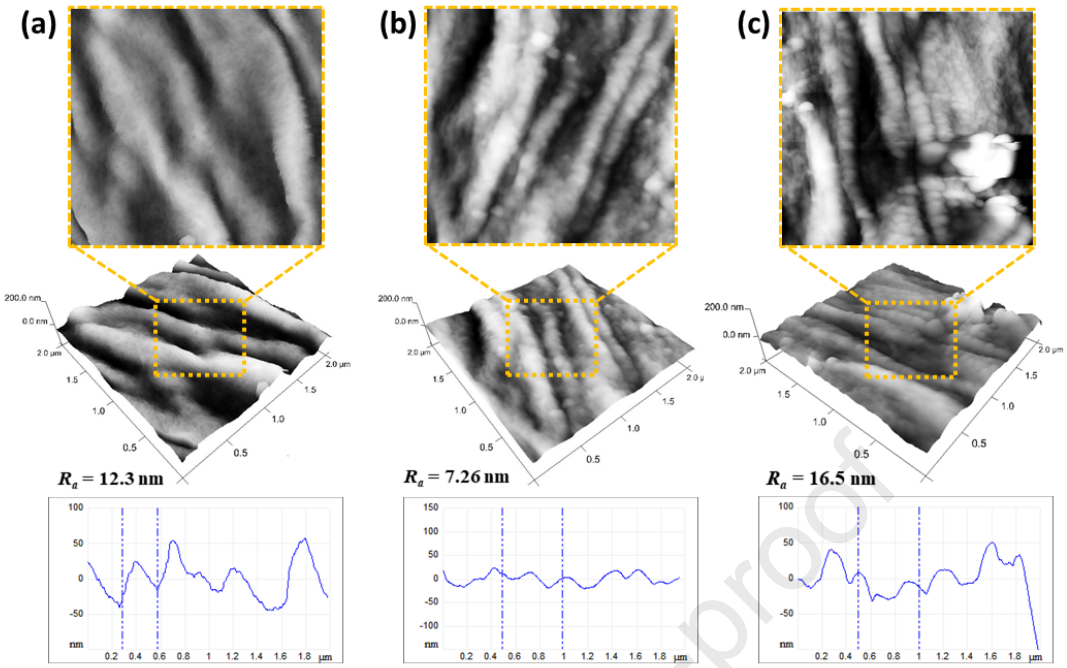

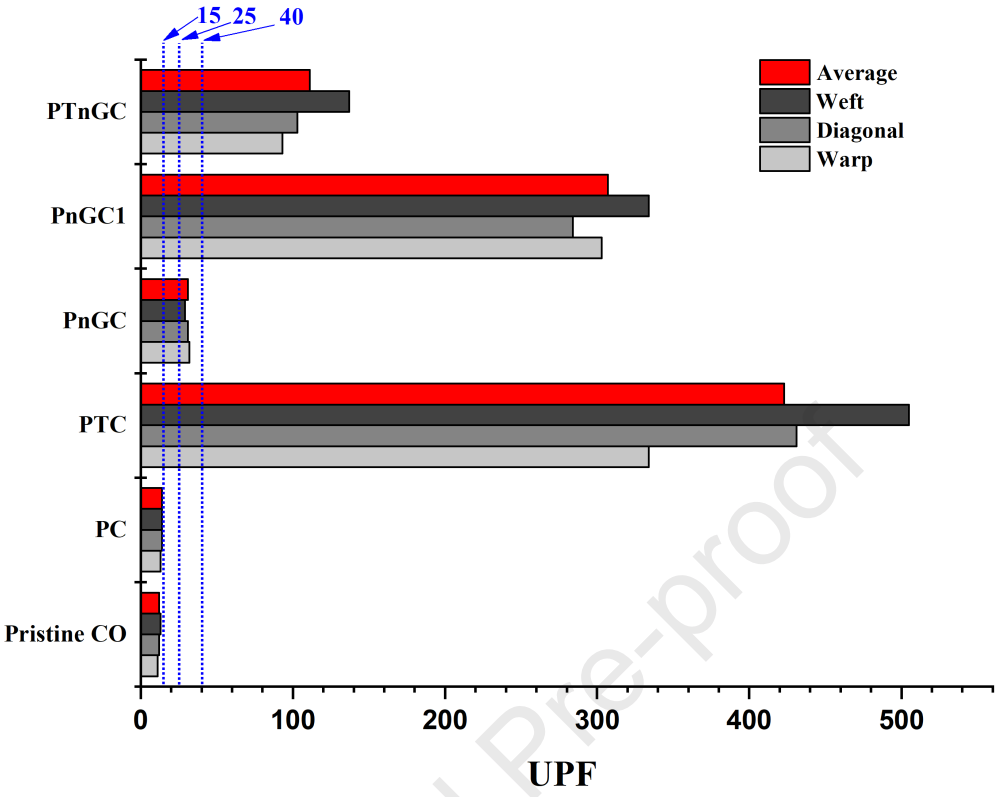

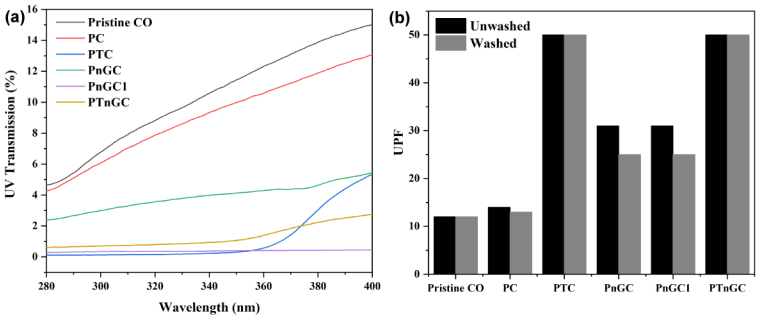

Declaration of interests

☒ The authors declare that they have no known competing financial interests or personal relationships that could have appeared to influence the work reported in this paper.

☐The authors declare the following financial interests/personal relationships which may be considered as potential competing interests: